Cell Reports

Report

The TFAM-to-mtDNA ratio defines inner-cellular nucleoid populations with distinct activity levels

Graphical abstract

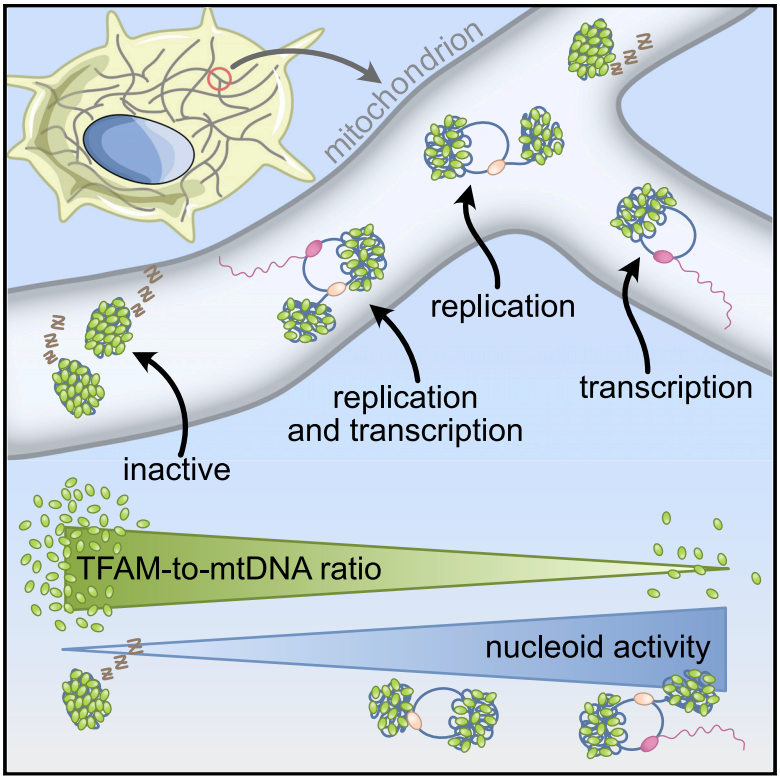

Authors

Christian Brüser, Jan Keller-Findeisen, Stefan Jakobs

Correspondence

sjakobs@gwdg.de

In brief

Brüser et al. report that the numerous nucleoids (mitochondrial DNA-protein complexes) located in the mitochondrial network of a single cell differ with respect to their replication and transcription activities. The study elucidates the role of mitochondrial DNA packaging in the regulation of mitochondrial transcription and replication.

Highlights

- A subset of human mitochondrial nucleoids is engaged in transcription and replication
- Active and inactive nucleoids form stable and coexisting populations in single cells
- TFAM-mediated DNA packaging controls transcription and replication in mitochondria
- Active and inactive nucleoids differ in size and shape

Brüser et al., 2021, Cell Reports *37*, 110000
November 23, 2021
https://doi.org/10.1016/j.celrep.2021.110000

CellPress

Cell Reports

CellPress
OPEN ACCESS

Report

The TFAM-to-mtDNA ratio defines inner-cellular nucleoid populations with distinct activity levels

Christian Brüser,[1,2] Jan Keller-Findeisen,[3] and Stefan Jakobs[1,2,4,5,6,*]

[1]Department of NanoBiophotonics, Research Group Mitochondrial Structure and Dynamics, Max Planck Institute for Biophysical Chemistry, 37077 Göttingen, Germany

[2]Clinic of Neurology, High Resolution Microscopy of the Cell, University Medical Center Göttingen, 37075 Göttingen, Germany

[3]Department of NanoBiophotonics, Max Planck Institute for Biophysical Chemistry, 37077 Göttingen, Germany

[4]Fraunhofer Institute for Translational Medicine and Pharmacology ITMP, Translational Neuroinflammation and Automated Microscopy, 37075 Göttingen, Germany

[5]Cluster of Excellence "Multiscale Bioimaging: from Molecular Machines to Networks of Excitable Cells" (MBExC), University of Göttingen, Göttingen, Germany

[6]Lead contact

*Correspondence: sjakobs@gwdg.de

https://doi.org/10.1016/j.celrep.2021.110000

SUMMARY

In human cells, generally a single mitochondrial DNA (mtDNA) is compacted into a nucleoprotein complex denoted the nucleoid. Each cell contains hundreds of nucleoids, which tend to cluster into small groups. It is unknown whether all nucleoids are equally involved in mtDNA replication and transcription or whether distinct nucleoid subpopulations exist. Here, we use multi-color STED super-resolution microscopy to determine the activity of individual nucleoids in primary human cells. We demonstrate that only a minority of all nucleoids are active. Active nucleoids are physically larger and tend to be involved in both replication and transcription. Inactivity correlates with a high ratio of the mitochondrial transcription factor A (TFAM) to the mtDNA of the individual nucleoid, suggesting that TFAM-induced nucleoid compaction regulates nucleoid replication and transcription activity *in vivo*. We propose that the stable population of highly compacted inactive nucleoids represents a storage pool of mtDNAs with a lower mutational load.

INTRODUCTION

Mitochondrial DNA (mtDNA) encodes essential proteins of the oxidative phosphorylation system, and mtDNA mutations are associated with numerous severe human diseases (Nunnari and Suomalainen, 2012; Park and Larsson, 2011). Human mtDNA encodes 13 proteins, 2 ribosomal RNAs, and 22 tRNAs. Typically, a single mtDNA interacts with proteins and is compacted into a structure termed nucleoid (Bogenhagen, 2012; Bonekamp and Larsson, 2018). The most abundant nucleoid protein is the mitochondrial transcription factor A (TFAM), a high-mobility-group box domain protein with functions in transcription activation, mtDNA compaction, and nucleoid maintenance (Farge et al., 2012; Kukat and Larsson, 2013; Murugesapillai et al., 2016). Numerous other proteins are associated with nucleoids, including components of the transcription and replication machinery (Bogenhagen et al., 2008; Falkenberg et al., 2007; Farge and Falkenberg, 2019). Cells contain typically several hundred up to a few thousand nucleoids. It is common for mtDNA mutations to affect only a subset of all nucleoids, a phenomenon called heteroplasmy (Stewart and Chinnery, 2021; Wallace, 2010). Somatic tissues may contain abundant mtDNA mutations that can be linked to neurological and cardiac diseases, as well as respiratory failures (Park and Larsson, 2011).

It is not known if in cells all nucleoids are functionally similar or if individual nucleoids are dedicated to replication or transcription and form functionally separated subpopulations. *In vitro* data showed that the ratio of TFAM to DNA influences the compaction of nucleoids and thereby also the activity of reconstituted nucleoids (Bonekamp and Larsson, 2018; Farge et al., 2014; Kukat et al., 2015). In mouse tissues, TFAM has been shown to act as a general repressor of mtDNA expression (Bonekamp et al., 2021). Strong overexpression of TFAM in mice increases the mtDNA copy number, whereas deletion of the *Tfam* gene is accompanied with a loss of mtDNA (Ekstrand et al., 2004; Larsson et al., 1998). However, if and how the TFAM/mtDNA ratio of an individual nucleoid affects its activity *in vivo* is unknown.

Previously, using diffraction-limited microscopy, individual nucleoids could not be reliably visualized in cells because of their small size of less than 100 nm and their tendency to cluster with each other (Kukat et al., 2011), potentially resulting in substantial errors in the inferred duplication and turnover rates of nucleoids. To accurately visualize individual replication and transcriptionally active nucleoids, we here relied on multicolor diffraction-unlimited STED super-resolution microscopy (Jakobs et al., 2020).

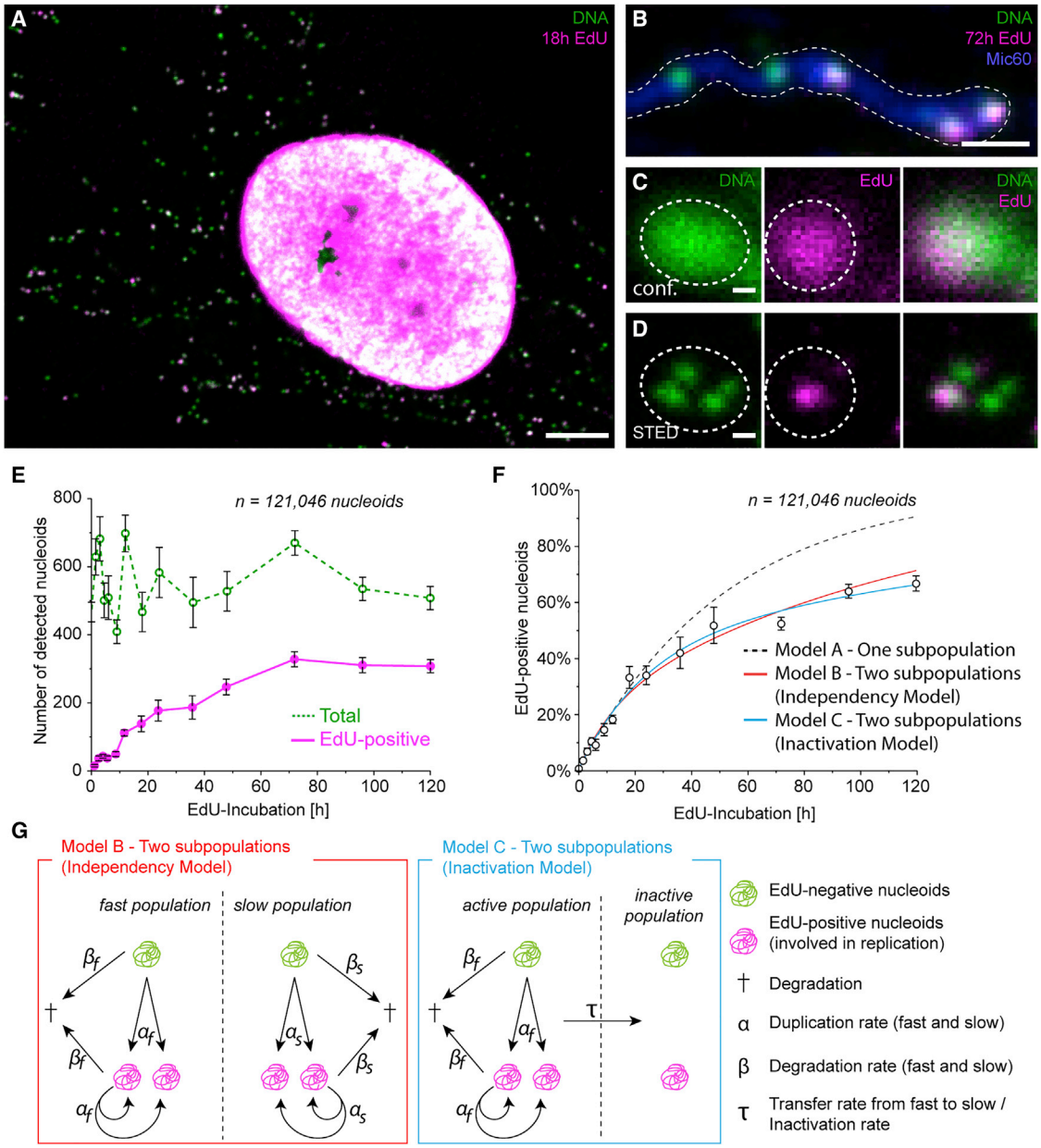

Figure 1. A large fraction of nucleoids is replication-inactive

(A) Primary HDFa cells were incubated for 18 h with EdU to label the replication-active nucleoids. Confocal image of an immunodecorated fibroblast. Green: DNA (all nucleoids); magenta: EdU-positive nucleoids.

(B) Replication-active and -inactive nucleoids are located in the same tubular mitochondrion after 72-h incubation with EdU. Green: DNA (all nucleoids); magenta: EdU-positive nucleoids; blue: mitochondrion (Mic60).

(C and D) STED super-resolution microscopy demonstrates that replication-active and inactive nucleoids can form a single cluster that is not resolvable by conventional microscopy. Color coding as before. (C) Diffraction-limited confocal recoding. (D) STED imaging.

(E) Number of EdU-positive nucleoids in a cell over time during incubation with EdU. The total number of nucleoids (green, dashed) and the total number of EdU-positive nucleoids (magenta) per cell were determined on STED images of 213 cells. See Figure S1 for the variation of the nucleoid content in single cells.

(F) Modeling of nucleoid dynamics. At least two nucleoid populations are required to explain the experimentally determined EdU incorporation dynamics. Shown are the best-fitting modeled EdU incorporation rates (for details on the parameters, see Table S1). Model A (dashed, black): all nucleoids are exhibiting the same duplication and degradation rates. Model B (independency model) (red line): two fully separated nucleoid populations with different activity levels. Model C (inactivation model) (blue): exchange between both populations is allowed, but the inactive population is entirely inert.

(G) Description of the two best-fitting models with only three variables. Left: model B (independency model), a population of active nucleoids exhibits high duplication (α_f) and degradation (β_f) rates. A second, less active population shows slower rates (α_s and β_s). The overall cellular nucleoid population size remains constant. The two populations do not exchange nucleoids. Model C (inactivation model): nucleoids can transfer from the active to the inactive population with a

RESULTS

A large fraction of nucleoids is replication inactive

For this study, we used early passage non-cancerous adult human dermal fibroblasts (HDFa) from healthy donors, because these cells are expected to contain fewer mutations in their mtDNA as compared with other cell models, such as cultivated cancer cells. We incubated these fibroblasts in 10 μM 5-ethynyl-2′-deoxyuridine (EdU). EdU is a synthetic nucleoside that incorporates after processing into newly synthesized nuclear and mtDNA during replication (Prole et al., 2020). The nucleoid-incorporated EdU was visualized in fixed cells by attaching a tag (Alexa Fluor 488) via click chemistry followed by indirect immunocytochemistry against the tag (Figure 1A). This approach increases the apparent size of the nucleoids by about 30 nm (Dyba et al., 2003) but has the benefit of increasing the signal-to-noise ratio strongly. The cells were additionally decorated with an antiserum against DNA to record the entire nucleoid population.

Nucleoids that were involved in mtDNA replication (EdU-positive nucleoids) and EdU-negative nucleoids localized in the same tubular mitochondrion (Figure 1B). STED super-resolution microscopy, but not diffraction-limited confocal microscopy, was able to visualize EdU-negative nucleoids clustering with EdU-positive nucleoids, demonstrating that the replication-inactive nucleoids are not spatially segregated from the replication-active nucleoids (Figures 1B–1D). We observed a strong variance of fluorescence intensities, reflecting the progression of EdU incorporation during replication, but did not find an increased number of nucleoids exhibiting a specific low-intensity fluorescence, which would potentially indicate a stable D-loop formation (Nicholls and Minczuk, 2014).

To determine the kinetics of nucleoid turnover, we kept the cells for up to 120 h in a medium containing a constant concentration of EdU and visualized the nucleoids that were involved in mtDNA replication after chemically fixing the cells at various time points after addition of EdU. Because generally an individual nucleoid contains a single mtDNA (Kukat et al., 2015), a nucleoid can be regarded as a "replication unit." Hence mtDNA replication and nucleoid duplication are coupled. To ensure a robust statistical analysis of nucleoid turnover, we analyzed more than 121,000 individual nucleoids in 213 cells. All analysis was performed semi-automatically in a blinded approach to avoid observer bias. The number of nucleoids per cell varied between around 200 and 1,000 (568 ± 223 [SD]), which presumably reflects different cell-cycle stages (Figure S1). The average number of nucleoids per cell fluctuated at around 568 ± 15 (SE) over the course of 5 days, suggesting that the EdU incubation had no influence on the nucleoid duplication and degradation dynamics (Figure 1E). Intriguingly, after 1 day, one-third of the nucleoid population was EdU positive, whereas even after 5 days, more than one-third of the nucleoids still had not been involved in replication. This suggests a pronounced heterogeneity in the duplication rates of the nucleoids of a cell.

To understand the underlying nucleoid turnover dynamics, we systematically modeled various scenarios and compared the calculated nucleoid population dynamics with the experimental data. For the modeling, we set the overall doubling of the entire nucleoid population to 7 days, which corresponds to the experimentally determined cell division rate. The simplest assumption, a homogeneous nucleoid population with constant degradation and duplication rates, could be excluded, because for no combination of duplication and degradation rates did the modeled outcome fit to the experimental results (Figure 1F). Likewise, the assumption of two distinct nucleoid populations with either identical degradation or identical duplication rates did not suffice to explain the data.

The minimal model to describe the progression of the labeling of nucleoids by EdU faithfully encompasses two nucleoid populations with three independent parameters. We identified two different two-nucleoid population models to fit to the data with high accuracy (Figure 1G). Both models predict a nucleoid population with a high duplication rate (more than 0.5 nucleoid duplication per nucleoid and per day) and a second nucleoid population with very limited or no duplications (for details on the predicted duplication and degradation dynamics, see Table S1). In both models, the less active (or inactive) nucleoid population represents at least 50% of the entire nucleoid population. The models differ in that one model, the "independency model," predicts the existence of two fully independent nucleoid populations, whereas the other model, the "inactivation model," allows nucleoids to transition between the two populations. In the "independency model," the population of almost inactive nucleoids is maintained in dividing cells by a low but existing rate of nucleoid duplications, whereas in the "inactivation model," the inactive nucleoid population is fueled by the transition of active nucleoids into inactive ones. Both models predict high turnover rates of active nucleoids (more than 0.3 nucleoid degradation per nucleoid and per day). Such a high turnover is required, because the models predict that the nucleoid duplication rates exceed the cellular division rate, fully in line with previous reports (Stewart and Chinnery, 2021). Conceptually, the two models are very similar and not mutually exclusive.

Because models with two nucleoid populations and only three variable parameters allow to explain the experimental data very well, more complex models with more variables would also fit the data. Thus, our data demonstrate that replication-active and (almost) replication-inactive nucleoids exist, but these represent not necessarily separated populations, because also nucleoids with intermediate activities may be present.

Replication-active nucleoids are also transcriptionally active

The mitochondrial RNA (mtRNA) polymerase POLRMT and the activation factors TFAM and TFB2M are required for mitochondrial transcription initiation (Falkenberg et al., 2002; Ringel et al., 2011; Shutt and Gray, 2006). Transcription can result in

rate constant τ. The inactive population exhibits neither duplication nor degradation. See Table S1 for detailed parameters of both models. Also in this model, the overall nucleoid population size remains constant. Data are represented as the mean, and error bars indicate the standard error (E and F). STED images display raw data with minimal background subtraction.
Scale bars, 2 μm (A and B); 100 nm (C and D). See also Figure S1 and Table S1.

mtRNA synthesis or in the generation of a replication primer, which starts subsequent DNA replication. Thereby, mtDNA replication is mechanistically linked to mitochondrial transcription (Agaronyan et al., 2015; Minczuk et al., 2011; Pham et al., 2006; Posse et al., 2015). Thus, we next investigated whether the replication-active nucleoid population also exhibits an enhanced transcription activity. To visualize mtDNA replication together with transcription at single-nucleoid resolution, we supplemented the cell culture medium with EdU, and additionally added the synthetic nucleoside 5-bromouridine (BrU). BrU is processed and subsequently incorporated into RNA during transcription and thereby labels mtRNA (Iborra et al., 2004). To visualize the incorporated BrU, we decorated the fixed cells with an anti-5-bromo-2′-deoxyuridine (anti-BrdU) antibody.

We found that when the cells were incubated for more than 1 h in BrU, the fluorescence signal was distributed across the entire mitochondrial network and could no longer be assigned to a specific nucleoid. This suggests that after synthesis, the labeled RNA is quickly detached from the nucleoid. We found that a 25-min pulse of BrU resulted in a distinct mtRNA labeling, so that the newly synthesized mtRNA could still be reliably assigned to an active nucleoid. Intriguingly, STED microscopy revealed that a BrU signal was generally adjacent to the mtDNA, whereas an EdU signal typically co-localized with the mtDNA. To label replication and transcriptionally active nucleoids, we incubated the fibroblasts initially for 45 min in EdU and then added BrU to the EdU-containing medium for a further 25 min. We recorded nucleoids by three-color STED super-resolution microscopy to detect simultaneously EdU, BrU, and DNA (Figures 2A and 2B). All four possible nucleoid activity states were observed: inactive nucleoids, i.e., DNA labeling only (Figure 2C); replication-active nucleoids, i.e., DNA labeling and EdU signal (Figure 2D); transcriptionally active nucleoids, i.e., DNA labeling and BrU signal (Figure 2E); and nucleoids involved in replication and in transcription (DNA, EdU, and BrU signal) (Figure 2F). Because nucleoids with different activity states were distributed throughout the mitochondrial network (Figure 2G; Figure S2A) and different activity states were found in clusters of nucleoids, we conclude that the distance of a nucleoid to the nucleus does not influence its probability to be involved in replication or transcription.

Of more than 18,000 analyzed nucleoids, 8.3% were EdU positive and 15.1% were BrU positive, and thus were engaged in replication or transcription, respectively (Figure 2H). Hence in fibroblasts, more nucleoids are engaged in transcription than in replication at a given time point.

We next questioned whether replication-active nucleoids are more likely to be involved in transcription than replication-inactive nucleoids. The notion that individual nucleoids are dedicated solely to either replication or transcription could immediately be excluded, because a sizable number of nucleoids (3.4%) were replication and transcriptionally active. If replication and transcription were fully independent, one would expect that in the investigated time frame about 1.3% ± 0.06% (SE) (the product of the percentage of the EdU-positive and BrU-positive nucleoids) were involved in both processes. The observed number is 2.3- to 2.8-fold higher (3.4% ± 0.15% [SE]), demonstrating that these processes are linked (Figure 2H). Nucleoids active in replication are significantly more likely to be involved also in transcription than replication-inactive nucleoids and vice versa (Figure 2I; Figure S2B).

The data show that in cells mtDNA replication and transcription are linked. We conclude that the replication-active population of nucleoids coincides with the transcriptionally active nucleoid population. This suggests that the same mechanisms regulate mtDNA replication and mitochondrial transcription activation and inactivation in cells.

Active nucleoids are enlarged and exhibit a lower TFAM-to-mtDNA ratio

Previous super-resolution studies showed that nucleoids typically have a slightly elongated form, but that also other shapes may exist (Brown et al., 2011; Kukat et al., 2011). It has been suggested that a nucleoids' ellipticity reflects its compaction, and that the more elongated shapes represent active nucleoids with a lower degree of compaction (Gustafsson et al., 2016). To test this hypothesis, we determined the overall brightness, size, and shape of active and non-active nucleoids on three-color STED images. Analysis of more than 15,000 nucleoids revealed that replication and transcriptionally active nucleoids exhibited an increase in the fluorescence intensity upon decoration with an anti-DNA antibody by 36% and 56%, respectively, compared with inactive nucleoids (Figure 2J). In EdU-positive, but not necessarily in BrU-positive, nucleoids, the actual mtDNA content is temporarily increased during the replication process. Hence the overall increase in brightness suggests that in active nucleoids the accessibility of the DNA to the antibody is increased. The increase of the brightness is accompanied with a 2D enlargement of active nucleoids, by ~15% and ~18% on STED images (Figures 2K and 2L; Figure S2C), which corresponds to a volume increase of ~21% and ~26%, assuming that nucleoids have the shape of prolate spheroids (Figure S2D) (Bonekamp and Larsson, 2018). In the fibroblasts, most nucleoids adopted an elongated shape. The ratio of the antibody decorated nucleoids' long to short axis was significantly increased in replication (109 nm × 67 nm) and transcriptionally active nucleoids (110 nm × 68 nm) over inactive nucleoids (100 nm × 64 nm), proving a more pronounced ellipticity in active nucleoids (Figures 2K and 2L; Figure S2E). Hence the overall increase in size, brightness, and ellipticity of active nucleoids implies that to facilitate mtDNA replication and transcription, the otherwise highly compacted nucleoids soften and enlarge.

In vitro, the TFAM:mtDNA ratio influences the compaction of nucleoids, and studies using reconstituted nucleoids demonstrated that the compaction level influences replication and transcription (Farge et al., 2012, 2014; Kukat et al., 2015; Kukat and Larsson, 2013). Hence we next analyzed whether in cells the active nucleoids have a different TFAM:mtDNA ratio than the inactive nucleoids.

Because currently, to the best of our knowledge, all suitable antibodies against TFAM and DNA are produced in mice, we could not label these targets using immunocytochemistry simultaneously with a sufficient signal-to-noise ratio. Therefore, we could not determine the TFAM:mtDNA ratio on the single-nucleoid level directly. To overcome this problem, we recorded cells labeled for TFAM and EdU or for DNA and EdU, respectively, at different time points after the addition of EdU. The

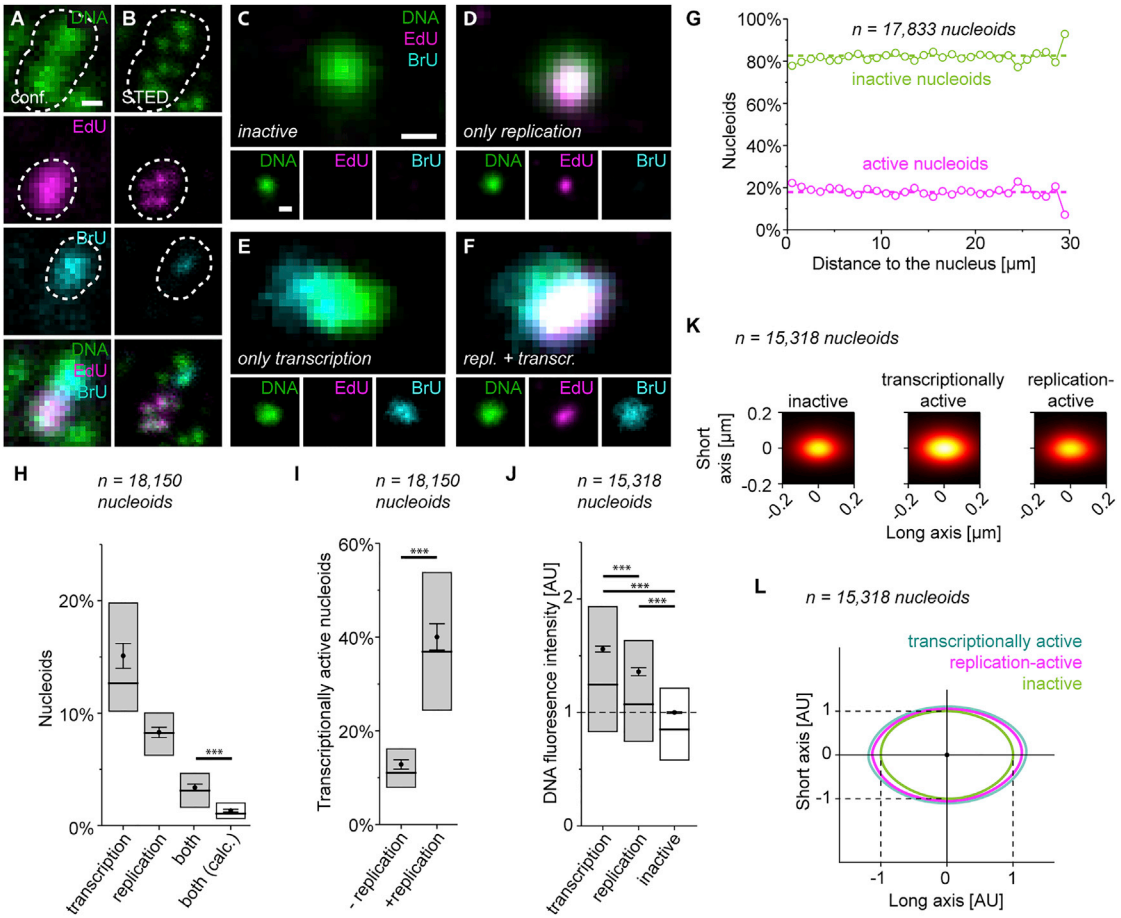

Figure 2. Replication-active nucleoids are also transcriptionally active

(A–F) Nucleoids can be involved in replication, transcription, or both processes. HDFa cells were incubated for 70 min with EdU to label replication-active nucleoids and for 25 min in BrU to label transcriptionally active nucleoids. Confocal (A) and STED (B–F) recordings of nucleoids of immunolabeled fibroblasts. Green: DNA (all nucleoids); magenta: EdU-positive nucleoids (replication); cyan: BrU-positive nucleoids (transcription). (A and B) Cluster of nucleoids with different activities resolved by STED microscopy. (C–F) Nucleoids with different activities.

(G) The activity of nucleoids is independent from their distance to the nucleus. The closest distance of the nucleoids of 51 cells to the surface of the respective nucleus was determined together with the activity status (replication and/or transcription) of the nucleoid.

(H) Fractions of nucleoids that were involved in replication or transcription within the preceding incubation period with EdU and BrU for 70 and 25 min, respectively. "both calc" indicates the mathematical product of the fractions of replication and transcriptionally active nucleoids; "both" shows the measured data.

(I) Replication-active nucleoids are more likely to be transcriptionally active than replication-inactive nucleoids.

(J) Transcription and replication-active nucleoids exhibit a higher DNA signal than inactive nucleoids.

(K) Averaged STED images of nucleoids immunolabeled for DNA. STED images of 12,375 inactive nucleoids, 2,228 transcriptionally active nucleoids, and 1,193 replication-active nucleoids were aligned and averaged.

(L) Active nucleoids are larger and show a more pronounced ellipticity. The contours of the averaged nucleoids shown in (K) were determined at their full width at half maximum (FWHM). The graphic displays the overlay of the contours normalized to the averaged inactive nucleoids. STED images were corrected for cross-talk. Note that the presented data depict the size of nucleoids decorated with antibodies. Boxplots show the inter-quartile range (25%–75%), the horizontal line represents the median, the dot represents the mean value, and error bars indicate the standard error (H–J).

Statistical significance was determined using two-tailed Student's t test; ***$p \leq 0.001$. The exact p values are given in Table S3 (H–J). Scale bars, 500 nm (A and B); 200 nm (C–F). See also Figure S2.

analysis revealed that at all time points, even within a single cell, the TFAM levels varied strongly between nucleoids, whereas the DNA signal per nucleoid varied only slightly (Figures 3A and 3B).

In order to calculate the average TFAM:mtDNA ratio in EdU-positive and EdU-negative nucleoids, we averaged the TFAM and the DNA fluorescence signal intensity of EdU-positive and EdU-negative nucleoids at each time point. We sampled at each time point between 10,000 and 20,000 nucleoids. Finally, the ratio between the average TFAM signal and the average DNA signal of the EdU-positive and the EdU-negative nucleoids, respectively, at the various time points was formed.

We found that already at 1.5 h, but also at prolonged incubations of 24 h with EdU, the average TFAM:mtDNA ratio was lower in EdU-positive nucleoids by 20%–40% compared with

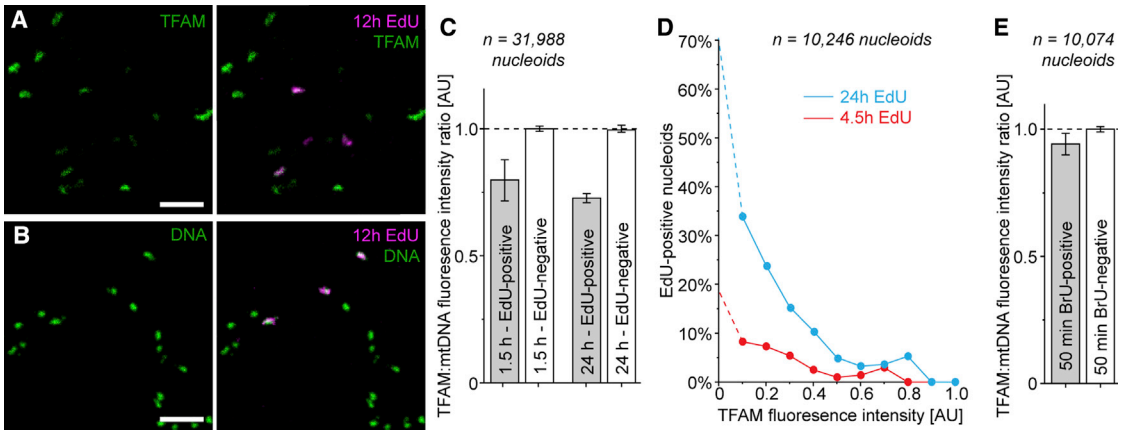

Figure 3. Active nucleoids exhibit a lower TFAM:mtDNA ratio

(A and B) Exemplary images of parts of fibroblasts, incubated with EdU for 12 h, and decorated for EdU and TFAM (A) or EdU and DNA (B).

(C) Replication-active nucleoids exhibit a reduced TFAM:mtDNA ratio. After 1.5- or 24-h EdU incubation, replication-active (EdU-positive) nucleoids show on average a 20% or 25% reduction of the TFAM:mtDNA ratio, compared with the respective inactive nucleoids. See also Figure S3 for different EdU incubation times.

(D) Low TFAM levels correlate with a high replication activity, as determined on the single-nucleoid level. Fibroblasts were incubated for 4.5 or 24 h with EdU and were subsequently labeled for EdU and TFAM. The TFAM signals of individual nucleoids measured on STED images were binned, and for each bin, the fraction of EdU-positive nucleoids was determined. The number of EdU-positive nucleoids in the bin with the lowest TFAM intensity (dashed line) was estimated based on a comparison of the different datasets to determine unspecific background.

(E) Transcriptionally active nucleoids exhibit a reduced TFAM:mtDNA ratio. After 50-min BrU incubation, transcriptionally active (BrU-positive) nucleoids show on average a 6% reduction of the TFAM:mtDNA ratio, compared with the respective inactive nucleoids. See Table S2 for the raw values of the TFAM and DNA fluorescence intensity.

Data are represented as the mean, and error bars indicate the standard error (C and E). Scale bars: 500 nm (A and B). See also Figure S1 and Table S2.

the EdU-negative nucleoid population (Figure 3C; Figure S3; Table S2). This suggests that in replicating nucleoids the mtDNA is decorated with less TFAM than in non-replicating nucleoids.

To further explore this finding, we determined the probability of a nucleoid with a specific TFAM level to be involved in replication at incubation times of 4.5 and 24 h (Figure 3D). For both time points, we found that nucleoids with low TFAM amounts had a higher probability to be replication active. This tendency was more obvious at longer incubations with EdU, presumably because after prolonged incubation with EdU also those nucleoids that belonged to the active population, but were involved in replication at a later time point, became EdU positive. Intriguingly, a large number of nucleoids (up to 35% of the EdU-positive nucleoids) had such a low TFAM signal that they escaped the automated analysis, because the TFAM signal was not or only slightly above the background noise. Because the EdU signal was highly specific, we could estimate the absolute numbers of nucleoids with very low TFAM levels (Figure 3D, dotted lines). We found that the nucleoids with very low TFAM levels exhibited a particularly high probability for mtDNA replication (Figure 3D).

Together this demonstrates that low TFAM levels indicate a high probability of replication, whereas high TFAM levels correlate with low replication rates. Nucleoids with very high TFAM levels did not show mtDNA replication activity, and nucleoids with very low TFAM levels exhibited a very high probability to be involved in replication.

Because our data show that replication and transcription are linked on the individual nucleoid level (Figure 2), this predicts that also transcriptionally active nucleoids exhibit a reduced TFAM:mtDNA ratio compared with transcriptionally inactive nucleoids. To test this hypothesis, we applied a 50-min BrU pulse, because this proved to be the longest incubation time that still allowed correlating the BrU signal to a specific nucleoid without excessive background. We found that in the BrU-positive nucleoids, the TFAM:mtDNA ratio was on average smaller by 6% compared with the BrU-negative nucleoids (Figure 3E; Table S2). We assume that this value underestimates the actual difference in the TFAM/mtDNA ratio between transcription-competent and transcription-incompetent nucleoids, because within a 50-min BrU pulse presumably only a small fraction of the transcription-competent nucleoids were labeled.

Altogether, the data show that active nucleoids are larger and exhibit less TFAM per mtDNA, suggesting that high TFAM levels result in a compaction of the nucleoids, thereby reducing their ability to be involved in replication or transcription. The specific TFAM:mtDNA ratio of the individual nucleoid may be regarded as a molecular switch, deciding whether the nucleoid is inactive or primed to be engaged in replication and transcription. Because the TFAM:mtDNA ratio varies strongly across the nucleoid population, stable active and inactive nucleoid populations are established in a cell.

DISCUSSION

Mutated and wild-type mtDNAs are coexisting in cells, which is referred to as heteroplasmy (Stewart and Chinnery, 2021; Wallace, 2010). Heteroplasmic mtDNA mutations can be maternally inherited, and strong evidence shows that the

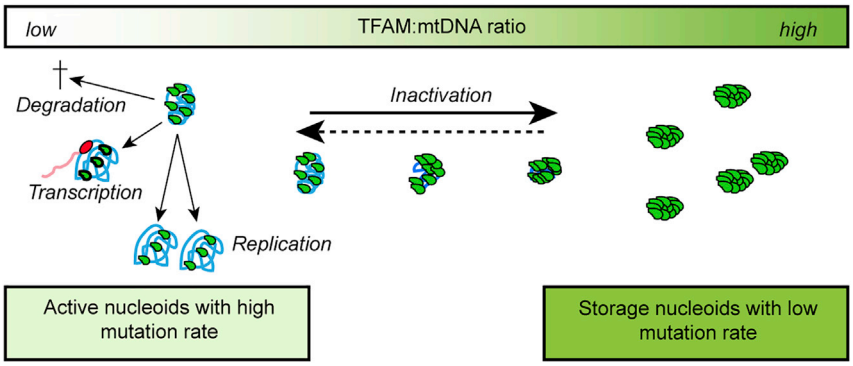

Figure 4. TFAM:mtDNA ratio of a nucleoid defines its activity level

Nucleoids with a low TFAM:mtDNA ratio exhibit high replication and transcription activity, whereas nucleoids with a high TFAM:mtDNA ratio are functionally inert. The sizable pool of inert nucleoids may contribute to keeping the mutational load of the mtDNA in somatic tissue low.

heteroplasmy level can change markedly between members of a pedigree (Cree et al., 2008; Wai et al., 2008). In addition to the inherited mtDNA mutations, increased levels of somatic mtDNA mutations have been observed in several diseases, as well as in aging humans. These somatic mutations tend to undergo clonal expansion that may cause mosaic respiratory chain deficiency in various tissues, causing a variety of phenotypes associated with aging and age-related diseases (Larsson, 2010). Presumably, mechanisms exist that counteract the expansion of mutated mtDNA in somatic cells, analogous to the genetic bottleneck described for the germline (Zhang et al., 2018). Whereas the genetic bottleneck hypothesis provides an explanation for the rapid changes in the spread of mutations observed during transmission from one generation to the next, the molecular mechanisms underlying the changes in allele frequency in somatic cells are poorly understood.

This study demonstrates the presence of active nucleoids that exhibit high duplication and turnover rates, as well as a sizable inactive population with low replication and transcription activity. Previous studies relying on the incorporation of ^{3}H-thymidine, BrdU, or EdU into mtDNA demonstrated that mtDNA replication is independent of the cell cycle (Bogenhagen and Clayton, 1977; Davis and Clayton, 1996; Gross et al., 1969; Kai et al., 2006; Lentz et al., 2010). These studies demonstrated variable turnover rates of nucleoids, with the average duplication and degradation rate depending on the cell type. These studies averaged across the entire nucleoid populations, because they could not resolve nucleoid subpopulations. When calculating the average duplication and turnover rates of a nucleoid population based on the determined single-nucleoid activity levels, we find nucleoid population dynamics comparable with those reported previously.

mtDNA replications are the major source of mtDNA mutations, because mtDNA replication induces point mutations, but also mtDNA deletions (Falkenberg and Gustafsson, 2020; Larsson, 2010; Phillips et al., 2017). In addition, the DNA repair mechanisms within mitochondria are less efficient than in the nucleus, which also contributes to an increased mutation rate in mtDNA compared with nuclear DNA (Fontana and Gahlon, 2020; Khrapko et al., 1997). Although the contribution of oxygen radicals to the overall generation of mtDNA mutations is controversially discussed (Larsson, 2010; Zheng et al., 2006), it is tempting to assume that the inactive, highly compacted nucleoids are protected by TFAM against the harsh mitochondrial environment (Alexeyev et al., 2013). Together this implies that the active nucleoid population is likely to be particularly vulnerable to the accumulation of mutations, whereas the inactive, highly compacted nucleoid population is comparatively well protected.

This raises the intriguing possibility that the inactive population serves as a storage pool of non-mutated mtDNAs (Figure 4). The data presented in this study support the concept that TFAM-induced compaction of nucleoids suppresses their replication and transcription activity. The TFAM:mtDNA ratio defines the active and non-active nucleoid populations, although the data do not exclude the possibility of more populations, or even a population gradient. To maintain the size of the inactive nucleoid population in dividing cells, the inactive nucleoids may either exhibit a low but existing duplication rate, or the population may be replenished by the transition of active nucleoids into inactive ones. Because the inactive nucleoids are presumably better protected against the accumulation of mutations, they may represent a storage pool of unmutated mtDNAs. Because the inactive nucleoids can be presumably activated by the removal of TFAM, mechanisms might exist that allow the cell to access the inactive nucleoid population upon mitochondrial damage or cell division.

Hence the finding of distinct nucleoid populations, which differ in activity and possibly in the mutational load, potentially opens up new avenues to investigate the genetic bottleneck both in the germline and in somatic tissues. The binding of TFAM to mtDNA, which apparently influences the balance between active and inactive nucleoids, may be influenced by regulating the TFAM levels or the affinity of TFAM to mtDNA (King et al., 2018; Matsushima et al., 2010).

In conclusion, we show that in cells at least two nucleoid populations with different transcription and replication activities exist, which are defined by the TFAM:mtDNA ratio of the individual nucleoid. This might open up strategies to devise novel pharmaceutical approaches targeting mtDNA diseases.

Limitations of the study

We investigated the ratio, dynamics, and structural properties of active and inactive nucleoids only in a single primary cell line (primary human dermal fibroblasts). The ratio of active to inactive nucleoids, as well as the exact replication and degradation dynamics, might differ in other cell types and more complex samples such as tissues.

STAR★METHODS

Detailed methods are provided in the online version of this paper and include the following:

- KEY RESOURCES TABLE
- RESOURCE AVAILABILITY
  - Lead contact
  - Materials availability
  - Data and code availability
- EXPERIMENTAL MODEL AND SUBJECT DETAILS
- METHOD DETAILS
  - Nucleoside incorporation
  - Immunolabeling
  - Microscopy
  - Nucleoid detection
  - Modeling of nucleoid population dynamics
  - No transfer between fast and slow population (Independency Model)
  - Transfer between a fast and a completely inactive population (Inactivation Model)
  - A single population
  - Colocalization of color channels
  - Calculation of nucleoids distance to the nucleus
- QUANTIFICATION AND STATISTICAL ANALYSIS

SUPPLEMENTAL INFORMATION

Supplemental information can be found online at https://doi.org/10.1016/j.celrep.2021.110000.

ACKNOWLEDGMENTS

We thank Nicole Molitor for excellent technical assistance. This work was supported by the Deutsche Forschungsgemeinschaft (DFG, German Research Foundation) under Germany's Excellence Strategy EXC 2067/1- 390729940 and by the European Research Council (ERCAdG No. 835102) (both to S.J.). It was funded by the DFG-funded SFB/TR 274 (project Z01 to S.J.).

AUTHOR CONTRIBUTIONS

C.B. and S.J. designed research. S.J. conceived the project. C.B. performed research. J.K.-F. performed the modeling. C.B., J.K.-F., and S.J. analyzed data. C.B. and S.J. wrote the paper. All authors approved the manuscript.

DECLARATION OF INTERESTS

The authors declare no competing interests.

Received: March 10, 2021
Revised: September 20, 2021
Accepted: October 22, 2021
Published: November 23, 2021

REFERENCES

Agaronyan, K., Morozov, Y.I., Anikin, M., and Temiakov, D. (2015). Mitochondrial biology. Replication-transcription switch in human mitochondria. Science *347*, 548–551.

Alexeyev, M., Shokolenko, I., Wilson, G., and LeDoux, S. (2013). The maintenance of mitochondrial DNA integrity—critical analysis and update. Cold Spring Harb. Perspect. Biol. *5*, a012641.

Bogenhagen, D.F. (2012). Mitochondrial DNA nucleoid structure. Biochim. Biophys. Acta *1819*, 914–920.

Bogenhagen, D., and Clayton, D.A. (1977). Mouse L cell mitochondrial DNA molecules are selected randomly for replication throughout the cell cycle. Cell *11*, 719–727.

Bogenhagen, D.F., Rousseau, D., and Burke, S. (2008). The layered structure of human mitochondrial DNA nucleoids. J. Biol. Chem. *283*, 3665–3675.

Bonekamp, N.A., and Larsson, N.G. (2018). SnapShot: Mitochondrial Nucleoid. Cell *172*, 388–388.e1.

Bonekamp, N.A., Jiang, M., Motori, E., Garcia Villegas, R., Koolmeister, C., Atanassov, I., Mesaros, A., Park, C.B., and Larsson, N.G. (2021). High levels of TFAM repress mammalian mitochondrial DNA transcription in vivo. Life Sci. Alliance *4*, e202101034.

Brown, T.A., Tkachuk, A.N., Shtengel, G., Kopek, B.G., Bogenhagen, D.F., Hess, H.F., and Clayton, D.A. (2011). Superresolution fluorescence imaging of mitochondrial nucleoids reveals their spatial range, limits, and membrane interaction. Mol. Cell. Biol. *31*, 4994–5010.

Cree, L.M., Samuels, D.C., de Sousa Lopes, S.C., Rajasimha, H.K., Wonnapinij, P., Mann, J.R., Dahl, H.H., and Chinnery, P.F. (2008). A reduction of mitochondrial DNA molecules during embryogenesis explains the rapid segregation of genotypes. Nat. Genet. *40*, 249–254.

Davis, A.F., and Clayton, D.A. (1996). In situ localization of mitochondrial DNA replication in intact mammalian cells. J. Cell Biol. *135*, 883–893.

Dyba, M., Jakobs, S., and Hell, S.W. (2003). Immunofluorescence stimulated emission depletion microscopy. Nat. Biotechnol. *21*, 1303–1304.

Ekstrand, M.I., Falkenberg, M., Rantanen, A., Park, C.B., Gaspari, M., Hultenby, K., Rustin, P., Gustafsson, C.M., and Larsson, N.G. (2004). Mitochondrial transcription factor A regulates mtDNA copy number in mammals. Hum. Mol. Genet. *13*, 935–944.

Falkenberg, M., and Gustafsson, C.M. (2020). Mammalian mitochondrial DNA replication and mechanisms of deletion formation. Crit. Rev. Biochem. Mol. Biol. *55*, 509–524.

Falkenberg, M., Gaspari, M., Rantanen, A., Trifunovic, A., Larsson, N.G., and Gustafsson, C.M. (2002). Mitochondrial transcription factors B1 and B2 activate transcription of human mtDNA. Nat. Genet. *31*, 289–294.

Falkenberg, M., Larsson, N.G., and Gustafsson, C.M. (2007). DNA replication and transcription in mammalian mitochondria. Annu. Rev. Biochem. *76*, 679–699.

Farge, G., and Falkenberg, M. (2019). Organization of DNA in Mammalian Mitochondria. Int. J. Mol. Sci. *20*, 2770.

Farge, G., Laurens, N., Broekmans, O.D., van den Wildenberg, S.M., Dekker, L.C., Gaspari, M., Gustafsson, C.M., Peterman, E.J., Falkenberg, M., and Wuite, G.J. (2012). Protein sliding and DNA denaturation are essential for DNA organization by human mitochondrial transcription factor A. Nat. Commun. *3*, 1013.

Farge, G., Mehmedovic, M., Baclayon, M., van den Wildenberg, S.M., Roos, W.H., Gustafsson, C.M., Wuite, G.J., and Falkenberg, M. (2014). In vitro-reconstituted nucleoids can block mitochondrial DNA replication and transcription. Cell Rep. *8*, 66–74.

Fontana, G.A., and Gahlon, H.L. (2020). Mechanisms of replication and repair in mitochondrial DNA deletion formation. Nucleic Acids Res. *48*, 11244–11258.

Gross, N.J., Getz, G.S., and Rabinowitz, M. (1969). Apparent turnover of mitochondrial deoxyribonucleic acid and mitochondrial phospholipids in the tissues of the rat. J. Biol. Chem. *244*, 1552–1562.

Gustafsson, C.M., Falkenberg, M., and Larsson, N.G. (2016). Maintenance and Expression of Mammalian Mitochondrial DNA. Annu. Rev. Biochem. *85*, 133–160.

Iborra, F.J., Kimura, H., and Cook, P.R. (2004). The functional organization of mitochondrial genomes in human cells. BMC Biol. *2*, 9.

Jakobs, S., Stephan, T., Ilgen, P., and Brüser, C. (2020). Light Microscopy of Mitochondria at the Nanoscale. Annu. Rev. Biophys. *49*, 289–308.

Kai, Y., Takamatsu, C., Tokuda, K., Okamoto, M., Irita, K., and Takahashi, S. (2006). Rapid and random turnover of mitochondrial DNA in rat hepatocytes of primary culture. Mitochondrion *6*, 299–304.

Khrapko, K., Coller, H.A., André, P.C., Li, X.C., Hanekamp, J.S., and Thilly, W.G. (1997). Mitochondrial mutational spectra in human cells and tissues. Proc. Natl. Acad. Sci. USA *94*, 13798–13803.

King, G.A., Hashemi Shabestari, M., Taris, K.H., Pandey, A.K., Venkatesh, S., Thilagavathi, J., Singh, K., Krishna Koppisetti, R., Temiakov, D., Roos, W.H., et al. (2018). Acetylation and phosphorylation of human TFAM regulate TFAM-DNA interactions via contrasting mechanisms. Nucleic Acids Res. *46*, 3633–3642.

Kukat, C., and Larsson, N.G. (2013). mtDNA makes a U-turn for the mitochondrial nucleoid. Trends Cell Biol. *23*, 457–463.

Kukat, C., Wurm, C.A., Spåhr, H., Falkenberg, M., Larsson, N.G., and Jakobs, S. (2011). Super-resolution microscopy reveals that mammalian mitochondrial nucleoids have a uniform size and frequently contain a single copy of mtDNA. Proc. Natl. Acad. Sci. USA *108*, 13534–13539.

Kukat, C., Davies, K.M., Wurm, C.A., Spåhr, H., Bonekamp, N.A., Kühl, I., Joos, F., Polosa, P.L., Park, C.B., Posse, V., et al. (2015). Cross-strand binding of TFAM to a single mtDNA molecule forms the mitochondrial nucleoid. Proc. Natl. Acad. Sci. USA *112*, 11288–11293.

Larsson, N.G. (2010). Somatic mitochondrial DNA mutations in mammalian aging. Annu. Rev. Biochem. *79*, 683–706.

Larsson, N.G., Wang, J., Wilhelmsson, H., Oldfors, A., Rustin, P., Lewandoski, M., Barsh, G.S., and Clayton, D.A. (1998). Mitochondrial transcription factor A is necessary for mtDNA maintenance and embryogenesis in mice. Nat. Genet. *18*, 231–236.

Lentz, S.I., Edwards, J.L., Backus, C., McLean, L.L., Haines, K.M., and Feldman, E.L. (2010). Mitochondrial DNA (mtDNA) biogenesis: visualization and duel incorporation of BrdU and EdU into newly synthesized mtDNA in vitro. J. Histochem. Cytochem. *58*, 207–218.

Matsushima, Y., Goto, Y., and Kaguni, L.S. (2010). Mitochondrial Lon protease regulates mitochondrial DNA copy number and transcription by selective degradation of mitochondrial transcription factor A (TFAM). Proc. Natl. Acad. Sci. USA *107*, 18410–18415.

Minczuk, M., He, J., Duch, A.M., Ettema, T.J., Chlebowski, A., Dzionek, K., Nijtmans, L.G., Huynen, M.A., and Holt, I.J. (2011). TEFM (c17orf42) is necessary for transcription of human mtDNA. Nucleic Acids Res. *39*, 4284–4299.

Murugesapillai, D., McCauley, M.J., Maher, L.J., 3rd, and Williams, M.C. (2016). Single-molecule studies of high-mobility group B architectural DNA bending proteins. Biophys. Rev. *9*, 17–40.

Nicholls, T.J., and Minczuk, M. (2014). In D-loop: 40 years of mitochondrial 7S DNA. Exp. Gerontol. *56*, 175–181.

Nunnari, J., and Suomalainen, A. (2012). Mitochondria: in sickness and in health. Cell *148*, 1145–1159.

Park, C.B., and Larsson, N.G. (2011). Mitochondrial DNA mutations in disease and aging. J. Cell Biol. *193*, 809–818.

Pham, X.H., Farge, G., Shi, Y., Gaspari, M., Gustafsson, C.M., and Falkenberg, M. (2006). Conserved sequence box II directs transcription termination and primer formation in mitochondria. J. Biol. Chem. *281*, 24647–24652.

Phillips, A.F., Millet, A.R., Tigano, M., Dubois, S.M., Crimmins, H., Babin, L., Charpentier, M., Piganeau, M., Brunet, E., and Sfeir, A. (2017). Single-Molecule Analysis of mtDNA Replication Uncovers the Basis of the Common Deletion. Mol. Cell *65*, 527–538.e6.

Posse, V., Shahzad, S., Falkenberg, M., Hällberg, B.M., and Gustafsson, C.M. (2015). TEFM is a potent stimulator of mitochondrial transcription elongation in vitro. Nucleic Acids Res. *43*, 2615–2624.

Prole, D.L., Chinnery, P.F., and Jones, N.S. (2020). Visualizing, quantifying, and manipulating mitochondrial DNA in vivo. J. Biol. Chem. *295*, 17588–17601.

Ringel, R., Sologub, M., Morozov, Y.I., Litonin, D., Cramer, P., and Temiakov, D. (2011). Structure of human mitochondrial RNA polymerase. Nature *478*, 269–273.

Shutt, T.E., and Gray, M.W. (2006). Bacteriophage origins of mitochondrial replication and transcription proteins. Trends Genet. *22*, 90–95.

Stewart, J.B., and Chinnery, P.F. (2021). Extreme heterogeneity of human mitochondrial DNA from organelles to populations. Nat. Rev. Genet. *22*, 106–118.

Wai, T., Teoli, D., and Shoubridge, E.A. (2008). The mitochondrial DNA genetic bottleneck results from replication of a subpopulation of genomes. Nat. Genet. *40*, 1484–1488.

Wallace, D.C. (2010). Mitochondrial DNA mutations in disease and aging. Environ. Mol. Mutagen. *51*, 440–450.

Zhang, H., Burr, S.P., and Chinnery, P.F. (2018). The mitochondrial DNA genetic bottleneck: inheritance and beyond. Essays Biochem. *62*, 225–234.

Zheng, W., Khrapko, K., Coller, H.A., Thilly, W.G., and Copeland, W.C. (2006). Origins of human mitochondrial point mutations as DNA polymerase gamma-mediated errors. Mutat. Res. *599*, 11–20.

STAR★METHODS

KEY RESOURCES TABLE

REAGENT or RESOURCE	SOURCE	IDENTIFIER
Antibodies		
anti-Mic60	Proteintech	Cat#10179-1-AP; RRID:AB_2127193
anti-dsDNA	Abcam	Cat#ab27156; RRID:AB_470907
anti-BrdU	Abcam	Cat#Ab6326; RRID:AB_305426
anti-TFAM	Abnova	Cat#H00007019-D01; RRID:AB_10717737
anti-Alexa Fluor 488	Thermo Fisher Scientific	Cat#A-11094; RRID:AB_221544
anti-rabbit	Jackson Immuno Research	Cat#111-005-144; RRID:AB_2337919
anti-mouse	Jackson Immuno Research	Cat#515-005-062; RRID:AB_2340288
anti-rat	Jackson Immuno Research	Cat#712-005-153; RRID:AB_2340631
anti-mouse-Alexa Fluor 594	Thermo Fisher Scientific	Cat#A-11032; RRID:AB_2534091
anti-rabbit-Alexa Fluor 594	Thermo Fisher Scientific	Cat#A-110337; RRID:AB_2534095
Chemicals, peptides, and recombinant proteins		
5-Bromouridine	Sigma Aldrich	Cat#858187
Abberior STAR RED (NHS carbonate)	Abberior	Cat#STRED-0002
Alexa Fluor 488 (NHS ester)	Thermo Fisher Scientific	Cat#A20000
Atto490ls (NHS ester)	Atto-Tec	Cat#AD 490ls-3
Critical commercial assays		
click-It EdU Cell Poliferation Kit for Imaging, Alexa Fluor 488 dye	Thermo Fisher Scientific	Cat#C10337
Deposited data		
Code	Zenodo	https://zenodo.org/record/5590223

RESOURCE AVAILABILITY

Lead contact

Further information and requests for resources and reagents should be directed to and will be fulfilled by the lead contact, Stefan Jakobs (sjakobs@gwdg.de)

Materials availability

This study did not generate new unique reagents.

Data and code availability

- All data reported in this paper will be shared by the lead contact upon request.
- All original code has been deposited at Zenodo and is publicly available as of the date of publication. DOIs are listed in the Key resources table.
- All raw data and additional information required to reanalyze the data reported in this paper are available from the lead contact upon reasonable request.

EXPERIMENTAL MODEL AND SUBJECT DETAILS

Adult human dermal fibroblasts of a male donor (American Type Culture Collection, Manassas, VA, USA, ATCC Number: PCS-201-012, Lot Nr: 70017799) were grown in Dulbecco's Modified Eagle Medium (DMEM) with glutaMAX and 4.5 g/L glucose (Thermo Fisher Scientific, Waltham, MA, USA), supplemented with 100 U/mL penicillin and 100 μg/mL streptomycin (Merck, Burlington, MA, USA), 1 mM sodium pyruvate (Sigma Aldrich, Munich, Germany) and 10% (v/v) fetal bovine serum (Merck) at 37°C and 5% CO_2. The fibroblasts were used before the 15th passage to ensure that the cells were not nearing the Hayflick limit.

METHOD DETAILS

Nucleoside incorporation

For labeling replication-active nucleoids, we used the click-It Alexa Fluor488 Kit (Thermo Fisher Scientific). Cells were incubated with 10 μM EdU between 70 min and 5 days. At incubation times of more than 12 h, the EdU containing medium was changed every 12 h to ensure a constant EdU concentration. When medium was changed, preconditioned medium supplemented with EdU was used. For the preparation of the preconditioned medium, fibroblasts were incubated in medium for at least 24 h and the medium was sterile filtrated before further use. For labeling transcriptionally active nucleoids, cells were incubated with 10 μM BrU (Sigma Aldrich) for 25 to 50 min. A 250 μM BrU solution in dH_2O was freshly prepared prior to each experiment.

Immunolabeling

For immunolabelling, cells were fixed with prewarmed (37°C) 4% formaldehyde in PBS (137 mM NaCl, 2.68 mM KCl and 10 mM Na_2HPO_4, pH 7.4) for 5 min at RT. If cells had been incubated with EdU or BrU, a short washing step with cell culture medium was performed prior to fixation. Fixed cells were extracted with 0.5% (v/v) Triton X-100 in PBS, blocked with 5% (w/v) BSA in PBS. If cells had been incubated with EdU, the incorporated EdU was labeled with Alexa Fluor 488 via a copper-catalyzed azide-alkyne cycloaddition (CuAAC) using the click-It Alexa Fluor 488 Kit according to manufacturers' instructions (Thermo Fisher Scientific). Afterward, cells were incubated with diluted primary antibodies against Mic60 (Proteintech, Rosemont, IL, USA), dsDNA (abcam, Cambridge, UK), BrdU (abcam), TFAM (Abnova, Thaipeh, Taiwan), or Alexa Fluor 488 (Thermo Fisher Scientific) in 5% (w/v) BSA in PBS for 1 h at RT. After washing in PBS, the primary antibodies were detected with secondary goat anti-rabbit, sheep anti-mouse or goat anti-rat antibodies (Jackson Immuno Research, Wes Grove, PA, USA) custom-labeled with Alexa Fluor 488 (Thermo Fisher Scientific), Atto490ls (Atto-Tec, Siegen, Germany), Abberior STAR RED (Abberior, Göttingen, Germany) or labeled by the manufacturer with Alexa Fluor 594 (Thermo Fisher Scientific). After washing with PBS, the cells were mounted in Mowiol with 0.1% 1,4-Diazabicyclo[2.2.2]octan (DABCO).

Microscopy

Confocal microscopy was performed with a TCS SP8 (Leica, Wetzlar, Germany) or with a STED 775 QUAD scanning microscope (Abberior Instruments, Göttingen, Germany) in the confocal mode. STED nanoscopy was performed using a STED 775 QUAD scanning microscope (Abberior Instruments) with either a 775 nm Katana-08 HP laser (Onefive GmbH, Regensdorf, Switzerland) or a 775 nm STED laser (Abberior Instruments) for stimulated depletion. The objective was an UPlanSApo 100x/1.40 Oil objective (Olympus, Tokyo, Japan). For STED nanoscopy, the fluorophore Atto490ls was excited at 485 nm, Alexa Fluor 594 was excited at 561 nm or 594 nm and Abberior STAR RED was excited at 640 nm. Images were recorded with a pixel size of 15 to 25 nm.

Nucleoid detection

Nucleoids were automatically segmented in two and three color 2D STED images. To this end, initially, the nucleus was identified by adding up all channel images, smoothing the result with a 2D Gaussian convolution kernel of variable width (~0.6 μm), binarizing the smoothed image with a variable threshold, morphologically filling holes in the binary structure and filtering out structures below a certain threshold area. Kernel width and binarizing threshold were chosen manually to optimally cover the nucleus.

The image areas outside the nucleus were smoothed (convolution with a 2D Gaussian of kernel width 150 nm) and background corrected (subtraction of 75% of the convolution with a 2D Gaussian of kernel width 0.6 μm). All spots above a certain threshold were taken as spot centers. This threshold was chosen manually after visual inspection (typically the threshold amounted to 10%–20% of the maximal signal value), to optimally include all nucleoid spots, but exclude false positive spots in the background. To each location a 2D elliptic, rotated Gaussian spot was fitted to the raw (unconvolved) data with a least-squares estimator. The fit results in background and signal amplitude, short and long axis as well as orientation. The ratio of long to short estimated axes of the fit gives the ellipticity. The brightness of a spot was estimated as the sum of raw image data in a circular region of 150 nm radius around the nucleoid location.

Modeling of nucleoid population dynamics

Nucleoids were modeled as belonging to two subpopulations - a slowly duplicating population with duplication rate α_s and degradation rate β_s and a fast duplicating population with duplication rate α_f and degradation rate β_f. Rates are assumed to be constant over time and adjusted so that the relative occurrence of the slow population is γ and that the total number of nucleoids doubles approximately every 7 days. Additionally, transfer between fast and slow populations is possible with a net transfer rate τ (can be positive or negative). Initially, all nucleoids are unlabeled and upon mtDNA replication both resulting nucleoids become labeled (EdU-positive) (Figure 1G). In the experiment, the fraction of labeled nucleoids over time is observed. By stating the problem as a system of ordinary differential equations and solving it, a theoretical model for the observed data is obtained. The two subpopulations are predicted to manifest themselves as two characteristic exponential decays with different amplitude and decay rates. We denote the slow populations with index s and the fast populations with index f, the unlabeled populations with index n (negative) and the labeled populations with index p (positive). The system of differential equations to solve is then:

$$\frac{dN_{sn}}{dt} = -(\alpha_s + \beta_s)N_{sn} + \tau N_{fn}$$

$$\frac{dN_{sp}}{dt} = 2\alpha_s N_{sn} + (\alpha_s - \beta_s)N_{sp} + \tau N_{fp} \quad (1)$$

$$\frac{dN_{fn}}{dt} = -(\alpha_f + \beta_f)N_{fn} - \tau N_{fn}$$

$$\frac{dN_{fp}}{dt} = 2\alpha_f N_{fn} + (\alpha_f - \beta_f)N_{fp} - \tau N_{fp}$$

The total number of nucleoids in a cell $N = N_{sn} + N_{sp} + N_{fn} + N_{fp}$ is expected to double after the average cell division time t_d. The initial conditions are $N_{sn}/N = \gamma$, $N_{fn}/N = 1 - \gamma$ and $N_{sp} = N_{fp} = 0$.

With the relative size of the slow and fast population fixed, the overall growth of the number of nucleoids is simply

$$N(t) = e^{(\gamma(\alpha_s - \beta_s) + (1-\gamma)(\alpha_f - \beta_f))t} = e^{ln2t/t_d} \quad (2)$$

which relates the population rates to the overall nucleoid doubling time. The number of nucleoids in the fast population can readily be solved by summing the two corresponding differential equations:

$$N_{fn}(t) + N_{fp}(t) = (1-\gamma)e^{(\alpha_f - \beta_f - \tau)t} = (1-\gamma)N(t) \quad (3)$$

which results in another rate constraint $\tau = \alpha_f - \beta_f - ln2/t_d$. The solution for N_{sn} is a bit more involved but an ansatz with a sum of two exponential functions results in

$$N_{sn}(t) = \frac{\gamma(\alpha_f + \beta_f) + \tau}{\alpha_f + \beta_f + \tau} e^{-(\alpha_s + \beta_s)t} - \frac{\tau(1-\gamma)}{\alpha_f + \beta_f + \tau} e^{-(\alpha_f + \beta_f + \tau)t} \quad (4)$$

The observed signal S, i.e., the fraction of positive (labeled) nucleoids, is conveniently computed by

$$S(t) = 1 - \frac{N_{sn}(t) + N_{fn}(t)}{N(t)} \quad (5)$$

and gives as the solution a sum of two exponentials:

$$S(t) = 1 - \frac{\gamma(\alpha_f + \beta_f) + \tau}{\alpha_f + \beta_f + \tau} e^{-(\alpha_s + \beta_s + ln2/t_d)t} - \frac{(1-\gamma)(\alpha_f + \beta_f)}{\alpha_f + \beta_f + \tau} e^{-(\alpha_f + \beta_f + \tau + ln2/t_d)t} \quad (6)$$

The solution to this general model has four free parameters and the experimental data did not allow estimating the parameter values of the general model with certainty. Therefore, further suitable constraints were introduced before weighted least-squares fitting of the solution to the data could be performed.

No transfer between fast and slow population (Independency Model)

If τ is set to zero, (6) reduces to

$$S(t) = 1 - \gamma e^{-2a_s t} - (1-\gamma)e^{-2\alpha_f t} \quad (7)$$

with $\beta_s = \alpha_s - ln2/t_d$ and $\beta_f = \alpha_f - ln2/t_d$.

Transfer between a fast and a completely inactive population (Inactivation Model)

For $\alpha_s = \beta_s = 0$, (6) reduces to

$$S(t) = 1 - \frac{2\alpha_f(\alpha_f - \beta_f - ln2/t_d)}{(\alpha_f - \beta_f)(2\alpha_f - ln2/t_d)} e^{-ln2t/t_d} - \frac{ln2/t_d(\alpha_f + \beta_f)}{(\alpha_f - \beta_f)(2\alpha_f - ln2/t_d)} e^{-2\alpha_f t} \quad (8)$$

with $\tau = \alpha_f - \beta_f - ln2/t_d$ and $\gamma = \tau/(\alpha_f - \beta_f)$.

A single population

The solution for a single population is trivially recovered if we set $\gamma = 1, \tau = 0, \alpha_s = \alpha, \beta_s = \beta$:

$$S(t) = 1 - e^{-2\alpha t} \quad (9)$$

with $\beta = \alpha - ln2/t_d$.

Colocalization of color channels

After detection of spots in each color channel, all other color channels were assigned to the DNA channel, which was supposed to contain all of the existing nucleoids. Iteratively, the EdU, BrU or TFAM spot that was closest to any DNA spot was found and together this pair was removed from the dataset, until the distance to the next available DNA spot was larger than a certain distance (0.1μm for EdU, 0.2μm for BrU). The found pairs were regarded as colocalized spots, the unpaired DNA spots were regarded as single DNA spots and unpaired EdU, BrU or TFAM spots (< 5% of all EdU, BrU or TFAM spots) were disregarded.

Calculation of nucleoids distance to the nucleus

The distance of a nucleoid to the nucleus was defined as the shortest distance to any edge of the detected nucleus in the 2D image. After colocalization of the color channels only the positions in the DNA channel were used for computing that distance.

QUANTIFICATION AND STATISTICAL ANALYSIS

Statistical analyzes in Figures 2H–2J and Figures S2B and S2C was performed with an unpaired two-tailed t test. The p values and a description of the compared datasets are listed in Table S3. All statistics were calculated using Origin 2017. Displayed diagrams were generated with Origin 2017, as well. Information on replicates, error bars, and statistical significance can be found in the figures and their corresponding legends.